Computers & Fluids 102 (2014) 266–276

Contents lists available at ScienceDirect

Computers & Fluids

journal homepage: www.elsevier.com/locate/compfluid

DSMC simulation of micro/nano flows using SBT–TAS technique

Ali Amiri-Jaghargh [a], Ehsan Roohi [a,*], Stefan Stefanov [b], Hassan Nami [a], Hamid Niazmand [a]

[a] High Performance Computing (HPC) Laboratory, Department of Mechanical Engineering, Faculty of Engineering, Ferdowsi University of Mashhad, P.O. Box 91775-1111, Mashhad, Iran
[b] Institute of Mechanics, Bulgarian Academy of Science, Acad. G. Bontchev Str., 1113 Sofia, Bulgaria

ARTICLE INFO

Article history:
Received 16 January 2014
Received in revised form 26 May 2014
Accepted 3 July 2014
Available online 12 July 2014

Keywords:
Micro/nano flows
DSMC
Simplified Bernoulli-trials (SBT) scheme
Transient adaptive subcell (TAS)
Memory reduction

ABSTRACT

The aim of the current work is to suggest a combination of the simplified Bernoulli-trials (SBT) collision algorithm with the transient adaptive subcell (TAS) technique implemented in the direct simulation Monte Carlo (DSMC) for calculation of non-equilibrium gas flows with reduced computational resources. In this work, we demonstrate that the use of the SBT collision scheme together with the TAS technique reduces the total number of particles (simulators), the number of grid cells and respectively, the computational memory, required for simulation of low Knudsen number micro/nano flows, while the accuracy is preserved. The efficiency of the SBT–TAS is investigated in details for two typical benchmark cases, namely, low Knudsen/low speed flow in a rectangular micro-cavity and high speed/high gradient flow over a nano-scale flat plate.

1. Introduction

The design and fabrication of micro/nano fluidic devices require enhanced understanding of flow dynamics and thermal phenomena in the non-equilibrium gas flows taking place in these devices, which have usually a complex geometry and often more than one characteristic length at micro/nanoscale. Based on the flow pressure and temperature, gaseous flow through micro/nano geometries could be considered as a non-equilibrium flow with different degrees of rarefaction; therefore, its numerical simulation cannot be performed by using conventional Navier–Stokes–Fourier (NSF) equations and a kinetic or direct molecular simulation must be applied. The Direct Simulation Monte Carlo (DSMC) method is such a particle-based algorithm for simulating rarefied gas flows [1]. The method is an accurate computational tool for the investigation of gas flows in regimes ranging from continuum to free-molecular conditions. The degree of gas rarefaction is determined by the Knudsen number, which is defined as the ratio of mean free path of gas molecules, λ, to a characteristic length, L, that is, $Kn = \lambda/L$. The rarefaction regimes can be generally categorized as slip ($0.001 < Kn < 0.1$), transition ($0.1 < Kn < 10$), and free molecular ($Kn > 10$) ones.

The DSMC method provides a reliable and accurate enough numerical simulation of the gas flow, but a disadvantage is that the method becomes time consuming at low speed or low Knudsen number flow regimes. The requirements for cell size, time step, and number of particles per cell lead to the significant restrictions on the traditional [1] and the modern DSMC methods. The standard DSMC algorithms require the cell size to be suitably smaller than one third of the gas mean free path and the time step should be small in comparison with the local mean collision time. Additionally, if the standard No Time Counter (NTC) collision scheme is applied, it should be at least 20 particles per cell to avoid repeated collisions and decrease the statistical fluctuations [2]. On the other hand, the recent DSMC algorithm requires dividing the numerical domain into collision and sampling cells [3] and recommends at least 7–8 particles to be used per collision cell for accurate collision modeling [2,4].

An alternative approach was proposed by Stefanov [5,6], who proposed a new "simplified Bernoulli trials (SBT)" collision scheme and showed that the SBT collision algorithm can provide accurate solutions even using 2 and often less than 2 particles per cell. The accuracy of the SBT scheme with few particles per cell was proved for a wide set of numerical problems in regimes from low speed/low Kn number to high speed/high gradient flows [7]. Our Previous investigation [7] has shown that the SBT scheme works more accurately compared with the majorant frequency (MFS) scheme [8] if a small number of particles, i.e., around 2 particles per cell, was employed in the simulation.

Although the SBT scheme works accurately with a small number of particles per cell, the same restriction as the mentioned previously on the grid size to be smaller than the mean free path makes DSMC codes based on the SBT scheme also time consuming,

* Corresponding author. Tel.: +98 (511) 8805136; fax: +98 (0511) 8763304.
E-mail address: e.roohi@ferdowsi.um.ac.ir (E. Roohi).

http://dx.doi.org/10.1016/j.compfluid.2014.07.003
0045-7930/

especially when concerning simulations at low Knudsen number micro/nano flows. In this regard, the current work presents the results of a combined SBT–TAS (transient adaptive subcells) DSMC solver that improves the efficiency of the simulation. The idea of transient adaptive subcell assumes a dynamic division of the sampling cells into subcells without keeping the information about the subcells all the time in computer memory. The idea of dynamic subdivision of collision cells was first suggested by Stefanov et al. [3]. They adjusted the subcell in such a way that subcell size remains smaller than mean free path at every time step. A division of the collision cell into adaptive subcells in such a way that a constant number of particles remains in the subcells was first suggested by Bird and implemented in the DS2V program [9]. This strategy was called transient adaptive subcell. Su et al. [10] extended the TAS technique for unstructured grids. They showed the advantage of TAS scheme application on a coarser unstructured grid and demonstrated a significant reduction of the required computational grid and time of the standard DSMC solver with "No Time Counter" (NTC) collision algorithm. In fact, TAS technique permits the grid resolution to adapt to the local flow gradient automatically. Additionally, it was shown that the computations by using TAS required low computer memory and low computational overhead [10]. Moreover, the TAS technique substantially improves the collision quality, which is defined as the ratio of mean collision separation (MCS) of the particles to mean free path (λ) [11,12].

In this work, a detailed analysis of the accuracy and computational time of the SBT–TAS algorithm is performed. To evaluate the suitability of the SBT–TAS algorithm in efficient prediction of low Knudsen micro/nano flows, rarefied flows in micro-cavity and over nanoscale flat plate geometry are considered in details. Effects of different parameters such as cell size, number of particles per cells/subcells and subcell grid movement are investigated.

2. Collision procedure

2.1. SBT algorithm

Recently, Stefanov [5] proposed the simplified Bernoulli trials (SBT) collision scheme as an alternative to NTC scheme that avoids the repeated collision in cells and permits simulations by using a small mean number of particles per cell, for example <PPC> ~ 2. In the SBT algorithm, the particles in the l^{th} cell are locally indexed in order to form a particle list numbered as $1 \ldots N^l$. The first particle of the collision pair (i, j), say i, is selected in strict order from the particle list, i.e., $i = 1 \ldots N^l - 1$. The second particle, say j, is then selected randomly among $k = N^l - i$ particles taking place in the list after particle i, i.e.

$$j = (i + 1) + int(k \times rnd) \tag{1}$$

where rnd stands for a random number between 0 and 1. Then each pair is checked for possible collision with the probability

$$p_{ij} = \frac{k f_{num} \Delta t \sigma_{ij} g_{ij}}{\forall^l} \tag{2}$$

where f_{num} is the ratio of real to the simulated number of particles, σ_{ij} and g_{ij} are respectively the collision cross-section and relative velocity of collision pairs i and j, and $\forall^l$ is the volume of the l^{th} cell. It should be noted that the time step Δt should be chosen in such a way so that p_{ij} rarely exceeds unity, say

$$prob\{p_{ij} \geqslant 1\} \to 0 \tag{3}$$

This procedure avoids the production of at least part of eventually repeated collisions [5]. For allowed repeated collisions in successive time steps that can be realized in SBT there are two possible answers-one mathematical and other physical: The first answer is based on the idea that the SBT algorithm was derived from the Kac collision model assuming a strict Markov collision process within a time step [6]. The stochastic collision process is built on the initial state, i.e., set of particle velocities in a cell at the beginning of each time step and the transition collision probabilities determined for each particle pair in a cell. After completing the collisions within a time step, a new state (velocity distribution) is formed that serves in the initial state for the collisions within the next step. At this moment, the step of particle free motion that changes the set of particles in the considered cell is neglected. It is obvious that it is not necessary to remember the past of the collision history. That is, the error realized by repeated collisions is included in the error of the Markov approximation of the collision process. In more detail, practically, the second answer is that at first exchange of particles between cells during the particle free motion occurs and second the probability of a collision of a given pair depends on the time step – the smaller time step leads to smaller probability for collision. The probability for a repeated collision is proportional to the product of probabilities $p_{ij} \times p_{ij}$. It can be shown that the order of the events is $O[(\Delta t)^2]$. Since the accuracy of the splitting scheme is $O(\Delta t)$ for small time steps Δt we can neglect the repeated collisions as introducing an error of higher order. Altogether with the particle free motion step this allows to neglect the effect of the repeated collisions realized in successive time steps.

In the NTC scheme, the situation is different, i.e., the decrease of time step leads to decrease of the maximum collision number in a collision cell within a time step. However, for a given particle pair the collision probability is determined by the acceptance–rejection rule with the probability $p = (\sigma g)/(\sigma g)_{\max}$ that does not depend on time step. Thus the probability for a repeated collision of a twice chosen pair in the NTC algorithm does not decrease with the decrease of time step. That is why, NTC codes must introduce a repeated collision preventing rule within more time steps.

Stefanov suggested another strategy that improves the SBT collision procedure: the usage of staggered (dual) grid [5]. Considering this approach, the SBT collision procedure is applied twice in two successive half-time steps on a dual grid. In the first half-time step, the collision algorithm is applied to the standard grid covering the computational domain while in the second half-time step, the collision algorithm is applied to a staggered grid, which is created by shifting all cells of the primary mesh in each coordinate direction by half-cell size, i.e., $\Delta x/2$, $\Delta y/2$. The use of dual grid makes possible in the second half-time step collisions of particles located at a separation distance smaller than a cell size, which belonged to different neighboring cells in the first half-time step. By translating the cells, they become particles of one cell and could be checked for a possible collision.

2.2. Transient adaptive subcell (TAS)

During the numerical simulation, particle density in different parts of the domain becomes non-uniform. For improving the quality of collisions, it is required that a finer grid is used in zones with higher particle density so that collision pairs could be selected more accurately. In this regards, it is suggested that subcell size dynamically adapts based on the number particle per cell, see Fig. 1.

Before reaching the steady state, the number of particles per cell varies during the computational process; consequently, the number of transient subcells also changes according to local density gradients. This dynamic subdivision was first employed in Ref. [3] and further modified and called transient adaptive subcell (TAS) by Bird [9]. To determine the number of subcells in each direction in a 2-D geometry, number of desired particles per

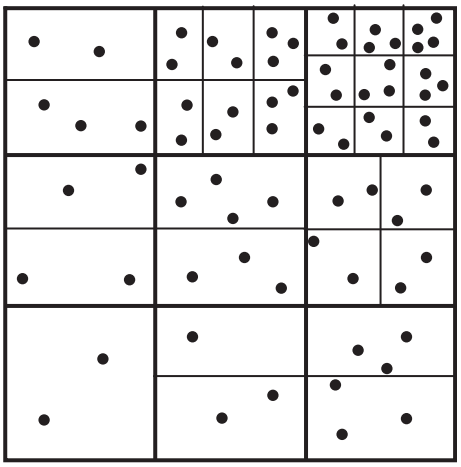

Fig. 1. TAS in cells with different PPC: Number of subcells in each cell is computed according to Eq. (4).

subcell, PPSC, should be set as one of the inputs. Since SBT algorithm performs the binary collision process accurately with 2 particles in mean, we considered PPSC = 2. To obtain a squared shape subcell grid, the number of subcells in x direction is calculated according to the following relation:

$$N_{SCX} = \sqrt{\frac{N_c}{PPSC \times AR}} \tag{4}$$

where N_c is the number of particles in the cell and $AR = \frac{\Delta y_{cell}}{\Delta x_{cell}}$. The number of subcell in y direction is $N_{SCY} = N_{SCX} \times AR + 1$ unless $N_{SCY} \times N_{SCX} > N_c/PPSC$, in this case $N_{SCY} = N_{SCX} \times AR$ is selected. The particles in the subcells are indexed in such order so that a sequential counting for using in the SBT scheme is attributed to the particles in each subcell that contains particles. This is the most complex part of applying the TAS technique for the SBT collision. After this indexing, the SBT collision algorithm given by Eqs. (1)–(3) is followed. Subcells volume, which now replaces the basic cell volume in collision probability given by Eq. (3), is calculated based on the volume of the basic cell and number of subcells.

Since the selection of collision pairs in the TAS technique is performed in subcells, the effect of cell-size on the accuracy of the solution is reduced and much coarser cells could be employed. The cell size is restricted by a condition that prevents of smearing of macroscopic gradients during the sampling stage. The accuracy of results can be improved if we displace the subcell grid. Subcell in each cell can be displaced in the same way as original cells, see Section 2.1.

2.3. SBT–TAS technique in DSMC algorithm

Once TAS technique is employed, sampling cell and collision cell become detached. Thus, the basic cell grid acts as a sampling grid that can be set as coarse as permitted while the quality of the binary collision process is controlled dynamically by settling of subcell grid. On the other hand, previous works [5,7] showed that computational efficiency of the SBT method decreases with increasing the number of particles in a collision cell. Using TAS technique, this issue is completely avoided because the transient adaptive subcells are set dynamically in such a way that the number of particles always remains limited.

During the simulation, the particle distribution in cells is not uniform; therefore, there may be subcells which are empty or contain only one particle. In this case, no collisions are possible in such cells. In the NTC–TAS approach suggested by Su et al. [10], if such a case occurs, usually a search through the neighboring subcells is performed to find a partner for collision pair. In the next sections, we will show that there is not a need to follow this procedure in SBT–TAS algorithm. Instead, we use two-half-time-step collision algorithm and shift the transient adaptive subcell grid in the second half-time step in order to prevent the reduction of collision frequency in the cell. By using a dual subcell grid, the single particles in cells within the first half-time step will have the chance to find a collision partner within the second half-time step. This is shown in the next subsection.

2.4. Displaced grid

One source of error in the DSMC method arises from the particles that are at a collision separation distance and have the potential to be selected as a collision pair, but they are not checked for collision as they are located in two neighboring cells. This difficulty may be overcome by using a dual grid that is created by translation of cells (or subcells). For an orthogonal grid, displaced grid can be created by translating cells in each axis direction by a distance equal to a half-cell size. Fig. 2 shows schematically the formation of the displaced grid. In this figure, solid lines show the main grid and dashed lines show the displaced grid that is obtained by displacing the main gird by a magnitude of $\Delta x/2$ in x direction and $\Delta y/2$ in y direction. It should be noted that the number of cells in the displaced grid is $(NCX + 1)(NCY + 1)$, where NCX and NCY are the number of cells in the original gird in x and y directions, respectively. Therefore, the volume of internal cells in the displaced grid is equal to the volume of internal cells in the main grid. However, the volume of boundary cells should be corrected. Fig. 2 also depicts two particles that despite being so close, they are not checked for collision since they are in two different cells in the main grid. After displacing the grid, these particles belong to one cell and collision possibility will be checked.

3. Results and discussions

To evaluate the ability of the SBT–TAS scheme to simulate efficiently near continuum rarefied flows, we considered low Reynolds flow in a micro cavity and high speed flow over a nano scale flat plate. We implemented the SBT–TAS collision scheme in an improved version of Bird's DSMC-2D code. The authors had already employed the above mentioned DSMC solver in different micro/nano flow applications, see Refs. [13–18]. In this work, molecular interactions are modeled using variable hard sphere (VHS) model and monatomic argon, $m = 6.63 \times 10{-}26$ kg and $d = 4.17 \times 10{-}10$ m, is considered as the gaseous medium.

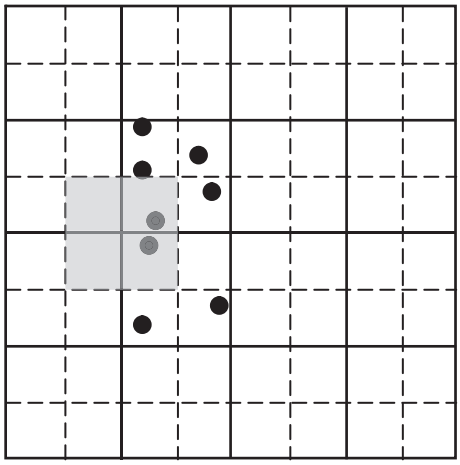

Fig. 2. Schematic of the displaced grid (dashed line), solid lines are the main grid, grey cell is a sample cell formed after grid movement.

3.1. Low speed flow in the cavity

3.1.1. Equilibrium collision frequency

In order to be sure that applying TAS technique does not reduce the collision frequency, first we study a flow in the equilibrium state. Equilibrium state in a cavity geometry is obtained if velocity of all walls is set equal to zero. In this state, the equilibrium collision rate per molecule (collision frequency) is given theoretically (CF_{th}) by [1]:

$$CF_{th} = 4nd^2\sqrt{\frac{\pi k_B T_{ref}}{m}}\left(\frac{T}{T_{ref}}\right)^{1-\omega} \tag{5}$$

where n, d, K_B, T_{ref}, m, and ω are number density, gas molecular diameter, Boltzmann constant, reference temperature, mass and viscosity–temperature exponent, respectively. To calculate this rate numerically, number of collisions in each cell are counted and divided by execution time and mean particle numbers per cell as follows:

$$CF_{num} = \frac{N_{coll}}{0.5\langle N_p\rangle Time} \tag{6}$$

Since two particles are engaged in a collision, coefficient 0.5 appears in the denominator. If SBT–TAS scheme is applied correctly, the ratio of the numeral value of CF to its theoretical value, CF_{Ratio}, should be equal to one.

The equilibrium collision frequency ratio of a cavity flow at $Kn = 0.005$, $T_w = 300$ K, simulated on a 25×25 grid using SBT–TAS technique, is shown in Fig. 3. If a fixed subcell grid is employed for this test, each cell side should be divided into 16 divisions so that the condition of $\Delta x_{coll} \leqslant \lambda/3$ becomes satisfied. Using TAS and assuming 2 particles per subcell, i.e., PPSC = 2, we set 512 particles per each cell; therefore, 16×16 subcells were obtained in each cell in average. As Fig. 3 shows, mean deviation of the equilibrium collision frequency ratio of one is in order of 10^{-4} and its maximum is about 0.2%. This proves that TAS technique is applied correctly and number of collisions in SBT–TAS scheme is accurate and coincides with the theory.

In our SBT–TAS scheme, adjacent subcells are not searched to find the collision pair, and collision is not applied in the cells that contain one particle or less. Therefore, there is a question that once the number of 'subcells containing one particle or no particle' increases, is SBT–TAS scheme able to provide correct collision frequency? To answer this question, the equilibrium collision frequency ratio in the cavity with 25×25 grid and 512 particles per cell (PPC), but with an average of 0.5 particles per subcell (PPSC), is considered. In this case, 32 subcells are made in each direction in average. Fig. 4 shows collision frequency ratio in this case. Similar to Fig. 3, mean deviation of the equilibrium collision frequency ratio of 1 is in order of 10^{-4} and its maximum is about 0.2%. Therefore, it is observed that SBT–TAS scheme is able to obtain the expected collision rate even without moving subcell grid.

3.1.2. Lid-driven cavity: 50×50 grid

At this stage, we consider SBT–TAS solution for lid-driven cavity flow at $Kn = 0.005$, $T_w = 300$ K and $U_{lid} = 100$ m/s. Without using TAS, a grid with 400×400 collision cells is required to satisfy cell size $<\lambda/3$ condition. Fig. 5 shows the temperature distribution along the vertical axis of the cavity. In this figure, SBT results in a 50×50 dual grid without TAS (SBT-Dual), with TAS but without dual grid (SBT–TAS), and with dual grid TAS (SBT–TAS-Dual) are shown. To validate the results, solution of the NTC model (without using TAS) obtained from a 200×200 grid with 2 fixed subcells in

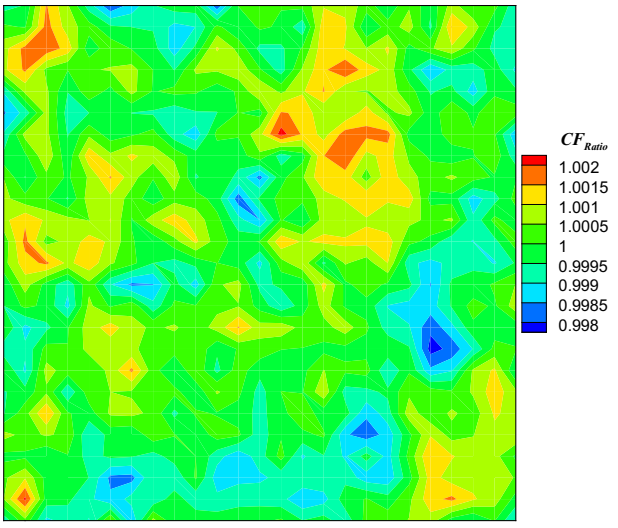

Fig. 4. Equilibrium collision frequency ratio in the cavity for a 25×25 grid with PPC = 512 and PPSC = 0.5.

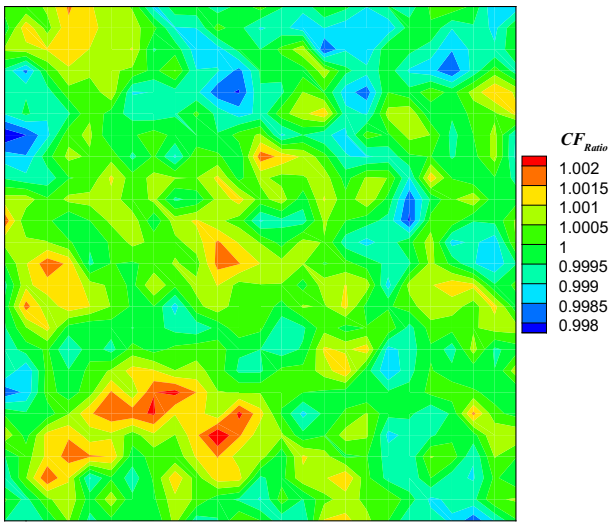

Fig. 3. Equilibrium collision frequency ratio in the cavity using a 25×25 grid with PPC = 512 and PPSC = 2.

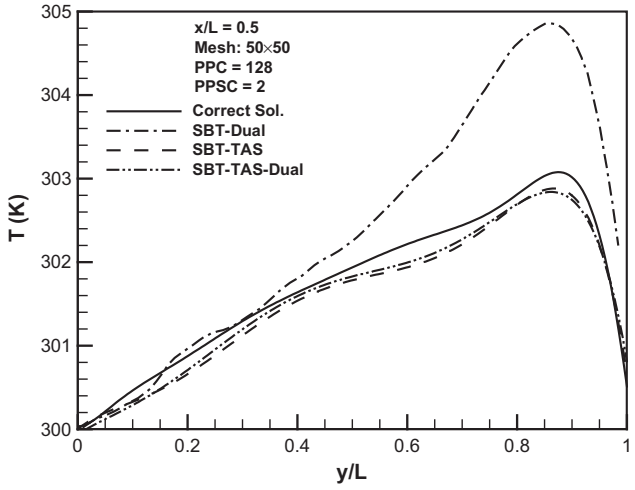

Fig. 5. Evaluation of SBT-Dual, SBT–TAS, SBT–TAS-Dual in prediction of the temperature profile in the cavity using a 50×50 grid.

each direction and 20 particles per cell was used (here called Correct solution).

To satisfy condition of: cell size $<\lambda/3$ in the 50×50 grid, it is necessary to divide each cell into 8 subcells in each direction in average. The TAS grid was obtained assuming two particles per each subcell. Therefore, according to the equation of subcell number, Eq. (4), it is necessary to put 128 particles per each cell. Fig. 5 shows that the solution of SBT-Dual, that is obtained using a 50×50 grid without TAS, deviates considerably from the Correct solution. This is expected as collision pairs are selected from a large cell. Using TAS, solutions approach to the correct one, with an error of 1% at the maximum temperature point. In this case, the implication of the dual grid slightly adds to the accuracy of the solution.

Fig. 6 shows the v-component of the velocity on the vertical axis of the cavity (Frame 6-a), u and v velocity components (Frames 6-b and 6-c) and temperature (Frame 6-d) on the horizontal axis of the cavity. The frames emphasize on the advantage of using SBT–TAS to obtain accurate solution using a coarse grid. They also show that dual grid technique slightly affects the accuracy of results. It should be considered that minor differences between SBT–TAS solution and the Correct solution may be due to smearing of local gradients during the sampling stage of the DSMC in a coarse 50×50 grid.

3.1.3. Lid-driven cavity: 25×25 grid

The SBT–TAS results obtained on a 25×25 grid in the cavity geometry (with the same initial/boundary condition as Section 3.1.2) are shown in Figs. 7 and 8. In Fig. 7, horizontal and vertical velocity components and temperature on the vertical axis of the cavity are shown. In Fig. 8, the same parameters are plotted on the horizontal axis. Compared to 50×50-grid, deviation of the results from the correct solution is slightly higher, however, the accuracy of SBT–TAS solution on 25×25 grid is almost acceptable. Considering temperature distribution graph, it is observed that moving subcell grid (SBT–TAS-Dual) enhances the accuracy of computations. Therefore, it is concluded that using TAS, main grid can be assumed quite coarse while the accuracy is nearly preserved.

Fig. 9 shows contours of the mean collision separation (MCS) normalized to the mean free path inside the cavity. This figure belongs to the solution over a 25×25 grid with PPC = 512. For pure SBT scheme in this coarse grid, the mean distance of selected pairs in all cells is more than twice of the mean free path of gas molecules. According to Fig. 9(b and c), using TAS technique makes MCS/λ less than 0.3 and 0.15 for SBT–TAS and SBT–TAS-Dual techniques, respectively.

Number of particles per subcell (PPSC) is another parameter that could be effective in the TAS performance. This parameter may have two opposing effects on the solution accuracy. First, if PPSC becomes small, cell will be divided into smaller subcells, and as a result, solution accuracy may improve due to decrease in the mean collision separation. However, this improvement is obtained with the cost of increasing the probability of creating subcells with only one particle. As our SBT–TAS algorithm does not search in adjacent subcells, this could reduce the accuracy of solutions.

Effect of decreasing PPSC on the mean collision separation for cavity flow using a 25×25 grid and 512 particles per cell is shown in Fig. 10. In this figure, upper row shows the SBT–TAS solution and the lower row depicts the results of SBT–TAS-Dual. The figure generally confirms that by decreasing the PPSC from 2 to 1, mean collision separation decreases. In the case of PPSC = 2, the average value of MCS/λ in SBT–TAS-Dual solution is about half of the corresponding value in the SBT–TAS solution. By further decreasing

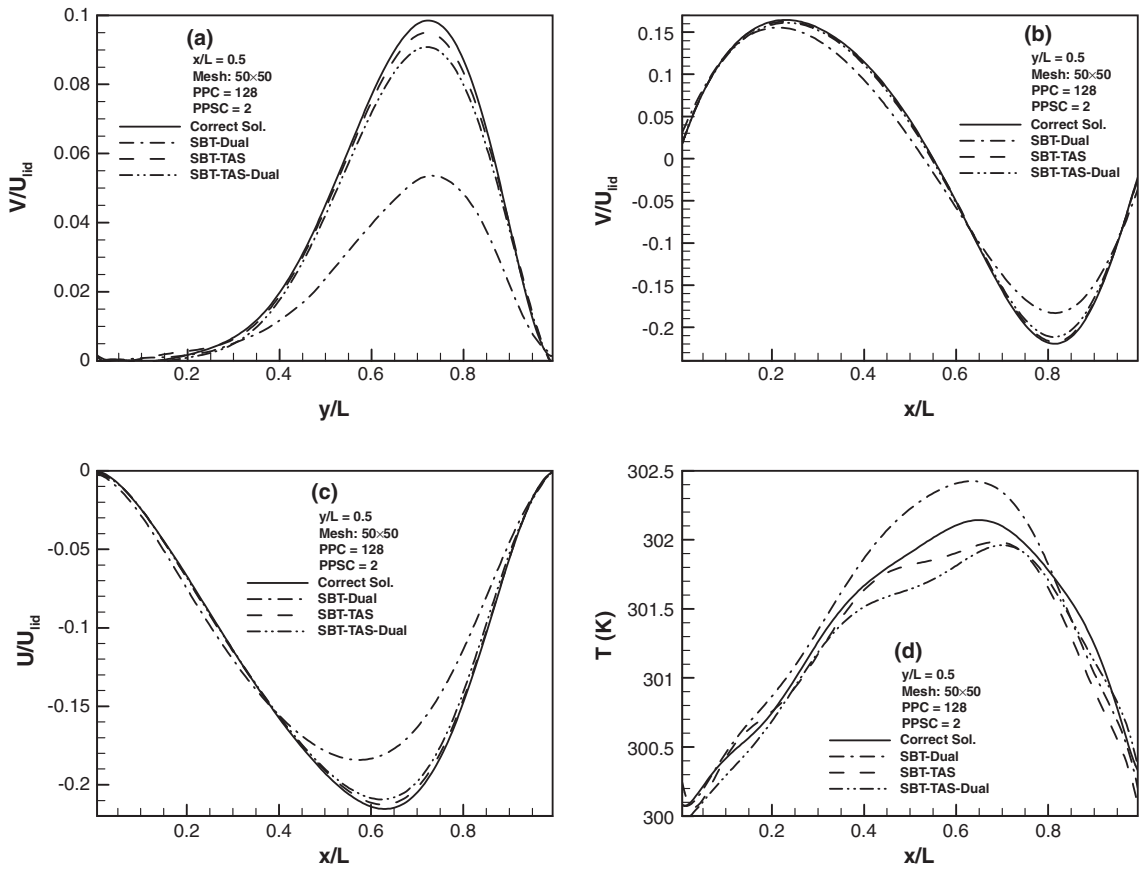

Fig. 6. Evaluation of SBT-Dual, SBT–TAS, SBT–TAS-Dual on improving DSMC results in the cavity using a 50×50 grid.

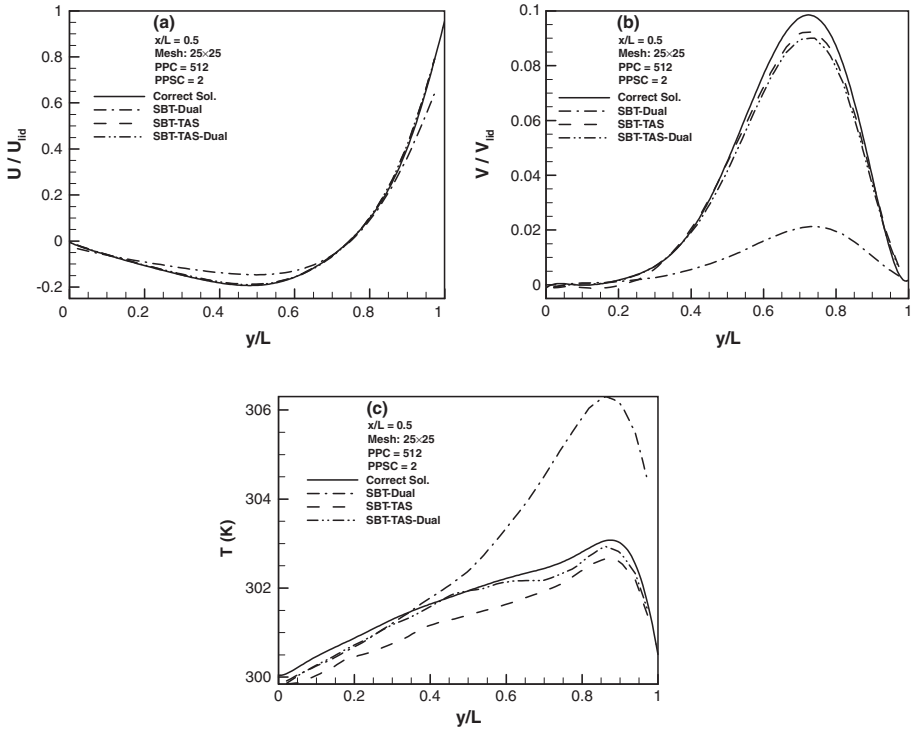

Fig. 7. Results of the TAS technique on the vertical axis of the cavity obtained using 25 × 25 grid-PPC = 512, PPSC = 0.5.

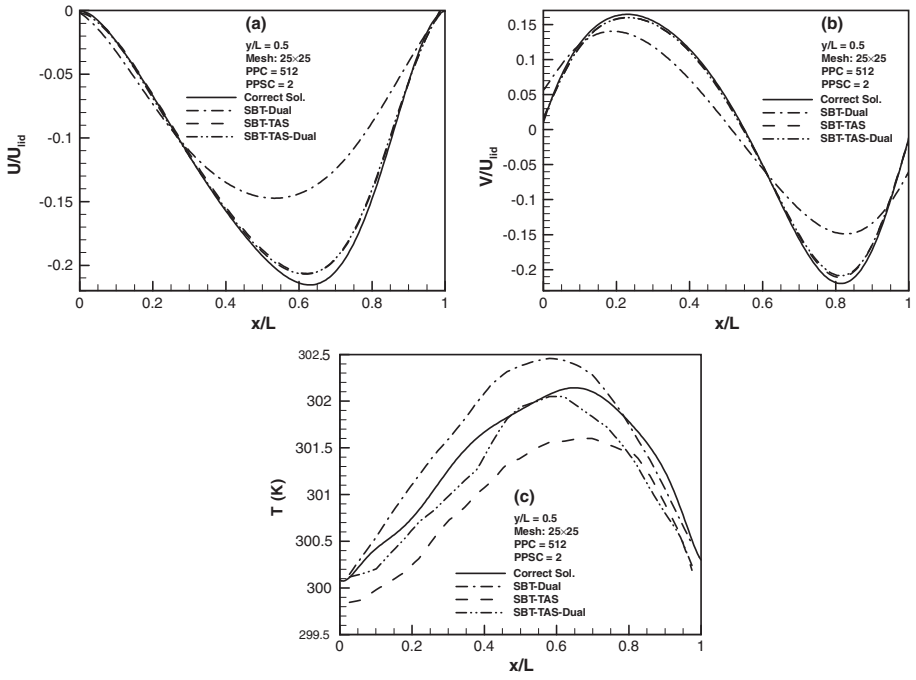

Fig. 8. Results of the TAS technique on the horizontal axis of the cavity obtained using 25 × 25 grid-PPC = 512, PPSC = 0.5.

PPSC from 1 to 0.5, the average amount of MCS/λ increases for SBT–TAS while it slightly decreases for SBT–TAS-Dual. Therefore, it could be concluded that PPSC = 1 is an optimal choice while the solution with PPSC = 2 remains within the limit of appropriate MCS/λ, which is smaller than 0.3 [4].

Fig. 11 shows the effects of the number of PPSC on the accuracy of the results of SBT–TAS technique (Frames 11(a) and 11(c)), and SBT–TAS-Dual technique (Frames 11(b) and 11(d)). The temperature profile on the vertical and the horizontal axis of the cavity are plotted. This figure shows that reduction of PPSC in SBT–TAS technique leads to an increase, and in SBT–TAS-Dual technique, it leads to a decrease of the accuracy of results. Similar graphs for the velocity components represent the same conclusion about PPSC effects in SBT–TAS and SBT–TAS-Dual. This observation

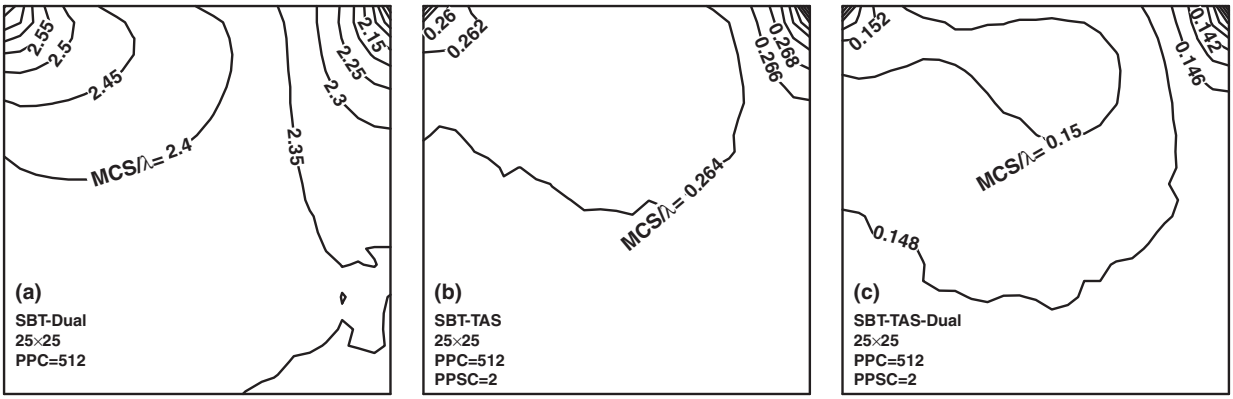

Fig. 9. Normalized mean collision separation in the cavity flow (a) SBT without applying TAS (b) SBT–TAS (c) SBT–TAS-Dual.

shows that any reduction in mean collision separation does not eventually result in an increase in accuracy [19]. As already mentioned, decreasing of the PPSC may correspond to more subcells with only 1 particle or less, where collision probability is not considered.

3.1.4. Computational efficiency

We already showed that coarser grids can be used in SBT–TAS without significant deviation from the benchmark (Correct) solution. This is beneficial in that it reduces a large amount of required computer memory. Relative computation time for the SBT–TAS technique in the cavity flow is reported in Table 1. The data are normalized with the required computation time for the standard (without TAS) NTC (Correct) solution. The required computation time for 50×50 and 25×25 grids, with PPSC = 2, is about 0.36 of the required time for the standard NTC solution (without TAS) and less than half of the computational time for SBT without TAS. Thus, application of TAS technique not only decreases the memory requirement, but also reduces the execution time appropriately. As execution time of 50×50 and 25×25 grids with PPSC = 2 are almost equal, using of the 50×50 grid is preferred as it provides more accurate output quantities. On the meanwhile, execution time decreases as PPSC decreases, while the accuracy of the solution increases in the case of the SBT–TAS. Table 1 shows that the computational time of the 25×25 grid with staggered (dual) subcells and PPSC = 0.5 is competitive with the 50×50 grid with PPSC = 2. Table 1 also indicates that the moving subcells grid adds 40% to the execution time while it does not have any signifi-

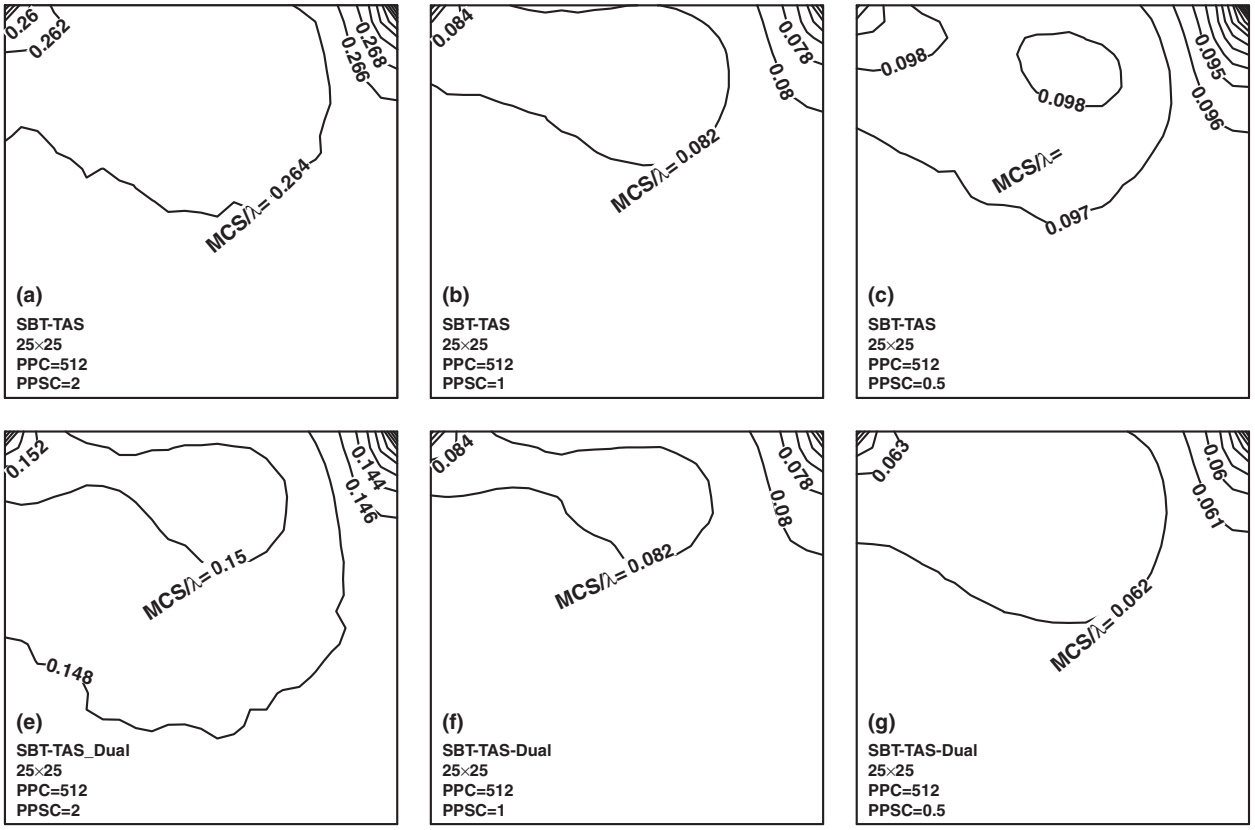

Fig. 10. Effect of particle number per subcell on the normalized mean collision separation.

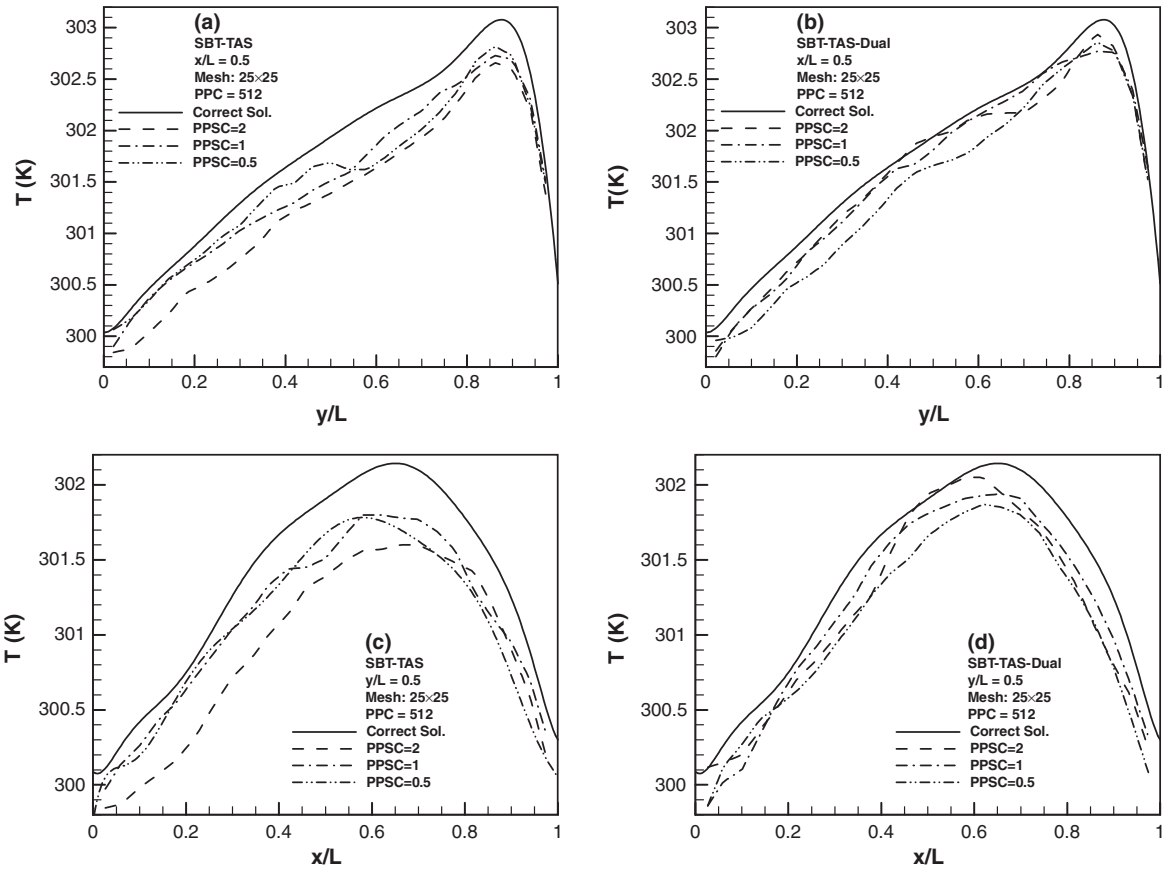

Fig. 11. Effects of particle number per subcell on the accuracy of the tempertaure profile, comparison of SBT–TAS and SBT–TAS-Dual.

cant effect on improving the results. Therefore, it seems that using the dual grid technique should be restricted to flows where such a small improvement in accuracy is critical.

Fig. 12 shows the average number of subcells in the cavity test with 25 × 25 grid and PPC = 512, PPSC = 0.5. The figure shows that the number of subcells in each region is different depending on the particle density in the flow. Particle density is proportional to the inverse of the local Knudsen number. Thus, it is expected that multiplication of the average subcells number by the local Knudsen remains nearly constant, see Fig. 13.

This constant number is approximately equal to the product of the global Knudsen number by the local subcells number, where the latter is given by Eq. (3).

$$Kn_{loc} \times \langle N_{SC} \rangle_{loc} \cong Kn \times N_{SC} = Kn \frac{PPC}{PPSC} \tag{7}$$

In this equation the Kn_{loc} stands for local Knudsen number which is the ratio of the local mean free path to the cavity length. We computed both sides of this equation, for different test conditions. As Table 2 shows, equality shown in Eq. (7) is almost verified.

Therefore, number of subcells per cell can be calculated directly from the following equation:

$$N_{SC} = \frac{Kn}{Kn_{loc}} \frac{PPC}{PPSC} \tag{8}$$

In this case, the number of subcells in each direction is the square of N_{SC}.

3.2. Supersonic flow over a nano-scale flat plate

Our second test case is the flat plate with the same boundary conditions as reported in Ref. [7]. The computational domain is a 100 × 60 nm rectangle. The length of the plate is considered as 90 nm and surface temperature is T_{wall} = 500 K. The flow passes over the plate with a free-stream velocity of 1412.5 m/s at the temperature of 300 K. The Knudsen number is Kn = 0.01 based on the plate length. Inlet, outlet and upper boundaries are considered as the free-stream boundary condition. To provide more realistic flow simulation, a specular wall boundary condition is applied to the first 10% of the domain at the upstream, see Fig. 14.

The computational domain is a 100 × 60 nm rectangle which contains a short section of 10% length of 10% specular wall boundary condition at the upstream of plate leading edge so that more realistic boundary conditions at the beginning of the plate is provided, see Fig. 14.

Table 1
Relative computation time of different techniques in the cavity flow.

Scheme	Grid	PPC	PPSC	Time
NTC	200 × 200	20	–	1
SBT-Dual	400 × 400	2	–	0.79
SBT–TAS	50 × 50	128	2	0.36
	25 × 25	512	2	0.36
	25 × 25	512	1	0.33
	25 × 25	512	0.5	0.28
SBT–TAS-Dual	50 × 50	128	2	0.51
	25 × 25	512	2	0.52
	25 × 25	512	1	0.47
	25 × 25	512	0.5	0.39

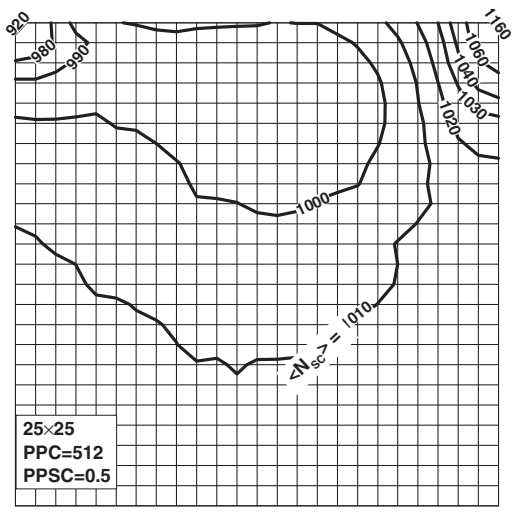

Fig. 12. Average of number of subcells in each cell in 25 × 25 grid with PPC = 512 and PPSC = 0.5.

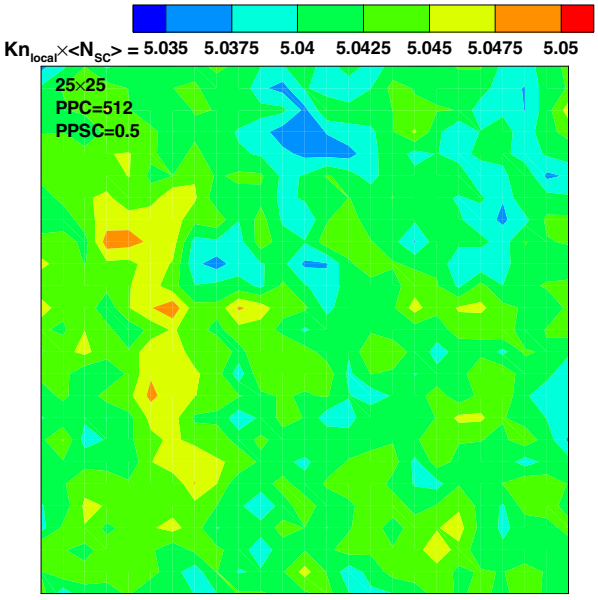

Fig. 13. Contour of local Knudsen number multiplied by the average subcells number.

Table 2
Evaluation of Eq. (7).

Grid	PPC	PPSC	$Kn_{loc}\langle N_{SC}\rangle_{loc}$	$Kn\frac{PPC}{PPSC}$
50 × 50	128	2	0.30	0.32
25 × 25	512	2	1.24	1.28
25 × 25	512	1	2.51	2.56
25 × 25	512	0.5	5.04	5.12
25 × 25	512	0.1	25.41	25.60
25 × 25	128	0.5	1.24	1.28

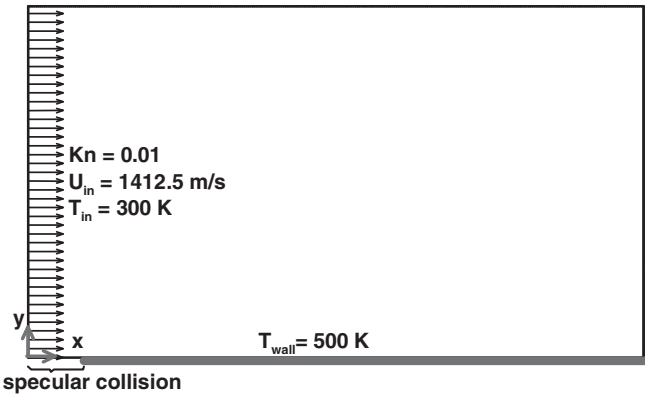

Fig. 14. Geometry and flow configuration for the nano-scale flat plate.

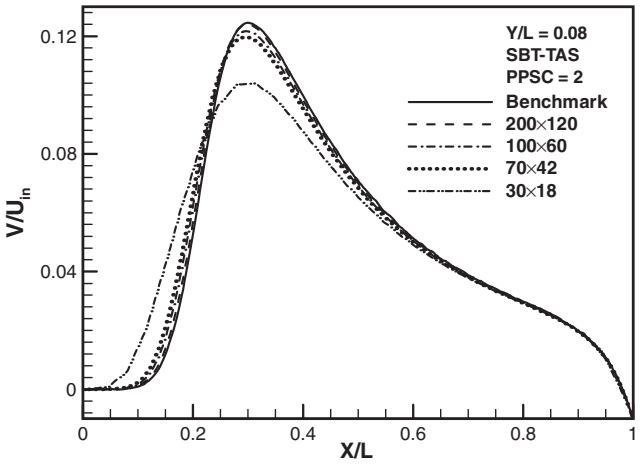

Fig. 15. Flow over the flat plate: SBT–TAS solutions compared with the benchmark NTC solution.

As we showed in Ref. [7], a mesh with 370 × 222 cell is the one which satisfies the grid size requirement (cell size < $\lambda/3$). In this section, we will show that using TAS technique permit us to use coarser grids without losing the accuracy. Fig. 15 shows the non-dimensional vertical velocity component along the line $Y/L = 0.08$ from different grids. Standard NTC solution (without TAS) with 370 × 222 grid and PPC = 20 is chosen as the benchmark solution. Additionally, SBT–TAS solution with PPSC = 2 is used with different grids. PPC is chosen in a way that the whole number of particles in the domain becomes approximately equal to 370 × 222 × 2, which is the total number of particles used in the SBT scheme. Therefore, particles per cell is 7, 28, 56, and 305 for 200 × 120, 42 × 60, 70 × 100, and 30 × 18 grid numbers, respectively. As Fig. 15 demonstrates, SBT–TAS solution on a 200 × 120 grid coincides with the benchmark. Additionally, SBT–TAS solution over the 70 × 42 grid, which is about 28 times coarser than the benchmark grid, is reasonably close to the benchmark solution, i.e., it has around 1% error at $X/L = 0.3$.

Fig. 16 shows the effect of applying TAS technique on improving the solution for temperature profile along the line $Y/L = 0.08$ and $Y/L = 0.2$. The results correspond to a grid with 70 × 42 cells. By applying the TAS technique, the deviation of SBT solution from the benchmark is reduced. It should be noted that temperature profile will coincide with the corresponding SBT–TAS profile if we apply dual subcells grid (SBT–TAS-Dual), thus, the latter is not shown here.

Shown in Fig. 17 is the mean collision separation in the cases with and without using TAS. The figure illustrates that mean collision separation is reduced to lower than 0.18 once TAS technique is applied. Changes in the flow parameters are considerable in the shock wave and boundary layer regions; therefore, if the sampling grid is not fine enough at these regions, the corresponding flow

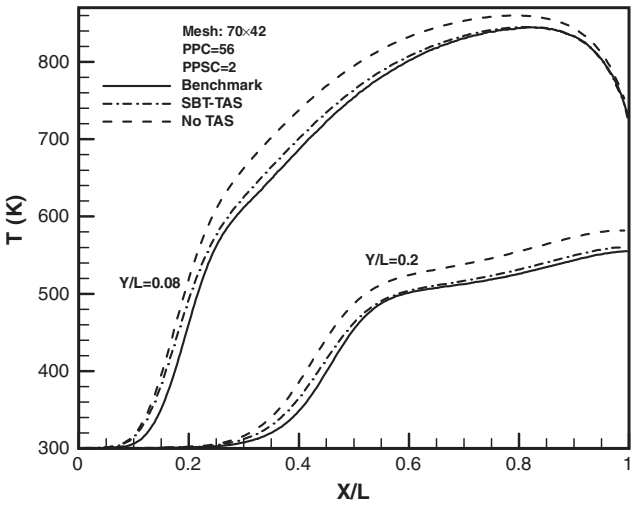

Fig. 16. Effect of using TAS technique for improving the results in 70 × 42 grid with PPC = 28 and PPC = 2 along the lines $Y/L = 0.08$ and $Y/L = 0.2$.

parameters would not be captured properly. This is more visible in the coarse grid with 30 × 18 cells. Fig. 15 showed that the results corresponding to this grid extremely deviate from the benchmark solution, while the mean collision separation in this case is around $\overline{MCS/\lambda} = 0.14$ in the whole domain.

Fig. 18(a) demonstrates that TAS technique makes the collision grid quite fine in the shock wave and boundary layer regions. In this figure, contours of average subcells per cell are plotted. The figure shows that in the region after the shock wave, where number density increases, collision grids are about 225 times finer than the sample grids, while this ratio is about 150 in the free stream region. Therefore, it can be concluded that TAS technique controls the collision grid suitably; however, if the changes in flow properties are considerable, i.e., shock wave region, coarse grids smear sharp flow gradients. Fig. 18(b) shows the contour of the product of the local Knudsen number by the mean subcells number. As is observed, this quantity is almost constant and fluctuates around its' average that is around 1.65.

3.2.1. Computational performance

Relative computational time for flow field solution over the flat plate is reported in Table 3. Execution time is normalized with respect to the benchmark solution time. Moreover, solution time is reported for the pure SBT without a TAS solution in 370 × 222 grid with PPC = 2. Sample size is the same for all cases reported in the table. Compared to the non-TAS solution, Table 3 shows that execution time decreases about 17% by applying the TAS technique in 70 × 42 grid. Even though the results of 200 × 120 grid coincide with the benchmark solution, it needs about 11% more computational time compared to the non-TAS solution, i.e., the advantage of TAS technique is restricted to the decreasing the required computers memory in this case.

Table 3
Relative computation time for TAS technique for the flow field solution over the flat plate.

Scheme	Grid	PPC	PPSC	Relative time
NTC	370 × 222	20	–	1
SBT-Dual	370 × 222	2	–	1.58
SBT–TAS	200 × 120	7	2	1.76
	100 × 60	28	2	1.38
	70 × 42	56	2	1.31
	30 × 18	305	2	1.26

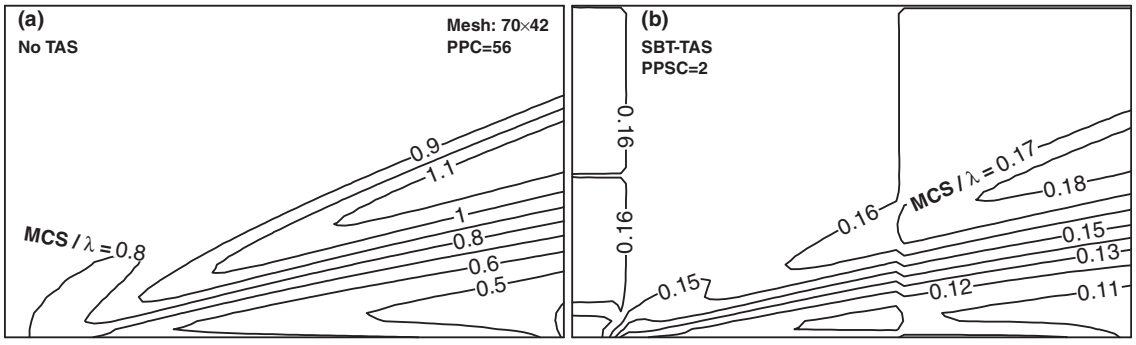

Fig. 17. Effect of using TAS technique on decreasing **MCS**/λ for the flat plate flow; Grid: 70 × 42, (a) without TAS (b) with TAS.

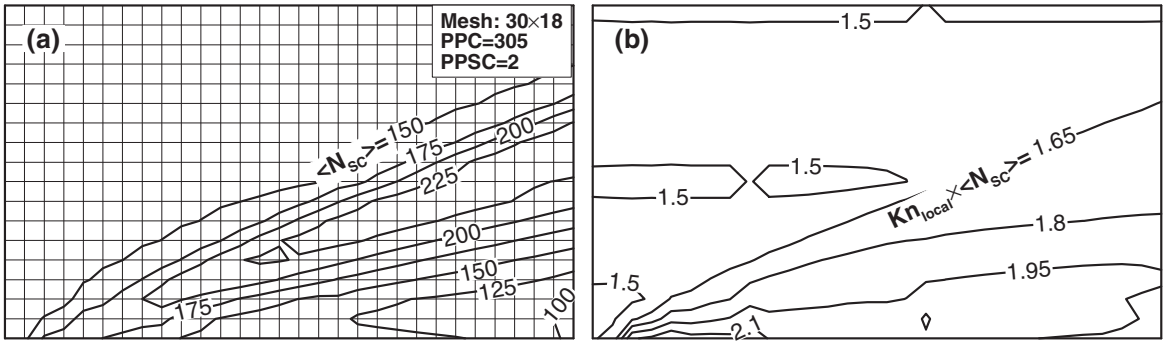

Fig. 18. Suitability of the TAS technique for controlling the collision in 30 × 180 grid with PPC = 305 and PPC = 2 (a) Average subcell numbers per cell ($\langle N_{SC} \rangle$), (b) product of local Knudsen number by the mean subcells number ($Kn_{local} \times \langle N_{SC} \rangle$).

4. Conclusions

In this work, we suggested a combination of the simplified Bernoulli trial (SBT) collision algorithm with the transient adaptive subcells (TAS) to simulate low Knudsen/low speed and low Knudsen/high gradient rarefied flows at micro/nano scales more efficiently. The main advantage of the proposed strategy is that it allows accurate DSMC calculations using a much smaller number of particles per subcell and coarser grid with less computation time compared to the standard NTC scheme. The TAS technique is not applied for the NTC scheme. We tested cavity flow at $Kn = 0.005$ and showed that our SBT–TAS solution using a coarse grid of 25×25 agrees suitably with the NTC solution using a 200×200 cell with 2×2 fixed subcells and PPC = 20, while the computational cost of the SBT–TAS is quite lower. We showed that using of TAS grid movement (SBT–TAS-Dual) decreases the mean collision separation while PPSC decreases; however, the extra computational cost of the grid movement is considerable and accuracy gain is not always guaranteed. We showed that the product of the local Knudsen number by the average subcells number in a cell remains constant and suggested an alternative formulation for N_{SC}, that is the number of subcell in each direction. For flow over the flat plate geometry, we showed that even though TAS scheme could provide enough number of collision subcells in coarse grids, the smearing of gradients due to a larger sample cell size could deteriorate the final solution.

Acknowledgments

The authors from the Ferdowsi University of Mashhad – Iran would like to acknowledge the financial supports provided by this University under Grant No. 28910. Stefan Stefanov would like to acknowledge the financial supports provided by Bulgarian NSF under Grant SuperCA++ – 2009 No DCVP 02/1.

References

[1] Bird GA. Molecular gas dynamics and the direct simulation of gas flows. Oxford, UK: Oxford University Press; 1994.
[2] Bird GA. Sophisticated DSMC. Notes prepared for a short course at the DSMC07 meeting, Santa Fe, USA; 2007.
[3] Stefanov SK, Boyd ID, Cai CP. Monte Carlo analysis of macroscopic fluctuations in a rarefied hypersonic flow around a cylinder. Phys Fluids 2000;12(5):1226–39.
[4] Bird GA. The DSMC method. USA: CreateSpace Independent Publishing Platform; 2013.
[5] Stefanov SK. On DSMC calculation of rarefied gas flow s with small number of particles in cells. SIAM J Sci Comput 2011;33(2):677–702.
[6] Stefanov SK. Particle Monte Carlo algorithms with small number of particles in grid cells in Numerical Methods and Applications. In: Dimov I, editor. Lecture notes in computer science, 6046; 2011. p. 110–7.
[7] Amiri-Jaghargh A, Roohi E, Niazmand H, Stefanov S. DSMC simulation of low knudsen micro/nanoflows using small number of particles per cells. ASME J Heat Transfer 2013;135(10):101008.
[8] Ivanov MS, Rogasinsky SV. Analysis of the numerical techniques of the direct simulation Monte Carlo method in the rarefied gas dynamics. Sov J Numer Anal Math Model 1988;3(6):453–65.
[9] Bird GA. The DS2V/3V program suite for DSMC calculations, Rarefied Gas Dynamics. 24th International symposium. American Institute of Physics, 762; 2005. p. 541–6.
[10] Su CC, Tseng KC, Cave HM, Wu JS, Lian YY, Kuo TC, Jermy MC. Implementation of a transient adaptive sub-cell module for the parallel-DSMC code using unstructured grids. Comput & Fluids 2010;39:1136–45.
[11] Gallis MA, Torczynski JR, Rader DJ, Bird GA. Convergence behavior of a new DSMC algorithm. J Comput Phys 2009;228(12):4532–48.
[12] Gallis MA, Torczynski JR. Efficient DSMC collision-partner selection schemes. AIP conference proceedings, 1333; 2011. p. 248–54.
[13] Akhlaghi H, Roohi E, Stefanov S. A New iterative wall heat flux specifying technique in dsmc for heating/cooling simulations of MEMS/NEMS. Int J Therm Sci 2012;59:111–25.
[14] Mohammadzadeh A, Roohi E, Niazmand H, Stefanov S, Myong RS. Thermal and second-law analysis of a micro- or nanocavity using direct-simulation Monte Carlo. Phys Rev E 2012;85:056305.
[15] Balaj M, Roohi E, Akhlaghi H, Myong RS. Investigation of convective heat transfer through constant wall heat flux micro/nano channels using DSMC. Int J Heat Mass Transf 2014;71:633–8.
[16] Mohammadzadeh A, Roohi E, Niazmand H. A parallel DSMC investigation of monatomic/diatomic gas flows in micro/nano cavity. Numer Heat Transfer, A: Appl 2013;63:305–25.
[17] Akhlaghi H, Roohi E. Mass flow rate prediction of pressure–temperature-driven gas flows through micro-/nanoscale channels. Continuum Mech Thermodyn 2014;26:67–78.
[18] Shoja-Sani A, Roohi E, Kahrom M, Stefanov S. Investigation of rarefied gas flow around NACA 0012 airfoils using DSMC and NS solvers. Eur J Mech: B: Fluid Mech 2014;48:59–74.
[19] Burt JM, Josyula E. Techniques for reducing collision separation in direct simulation Monte Carlo calculations. 42nd AIAA thermophysics conference, Honolulu, Hawaii; 2011.